NEAR SURFACE IN SITU STRESS PATTERN ADJACENT TO THE SAN ANDREAS FAULT, PALMDALE, CALIFORNIA

T. ENGELDER Lamont-Doherty Geological Observatory of Columbia University, Palisades, New York 10964
M. L. SBAR Department of Geosciences, University of Arizona, Tucson, Arizona 85721
S. MARSHAK Department of Geosciences, University of Arizona, Tucson, Arizona 85721
R. PLUMB Department of Geological Sciences and Lamont-Doherty Geological Observatory of Columbia University, Palisades, New York 10964

ABSTRACT

We made 29 in situ strain relaxation measurements distributed among eight sites spaced on a 35 km transect across the San Andreas fault and into the western Mojave desert southeast of Palmdale, California. Strain was measured by overcoring strain gauge rosettes bonded to the flattened bottom of boreholes. Our purpose was to measure the regional stress field and any modification of it by the San Andreas fault system. At our sites most distant from the fault we found NNE trending maximum compressive stress (σ_1) which is parallel to the σ_1 inferred from fault-plane solutions in southern California. There appears to be a clockwise rotation of σ_1 from NNE to approximately east-west on the north side of the fault. On the south side of the fault, σ_1 varies from N60°W to NNE. Along the 35 km transect σ_1 varied from 2.5 b to 32.9 b.

INTRODUCTION

This paper reports the results of a pilot study designed to test whether in situ strain relaxation measurements can detect the detailed tectonic stress field in the vicinity of a locked fault with a high rupture potential such as along the 1857 break of the San Andreas fault near Palmdale, California. Prescott and Savage (11) have shown that shear strain is accumulating in a right-lateral sense at a rate of 0.2 microstrain/year over a 10 to 15 km aperture across the fault near Palmdale. Yet data from small aperture triangulation nets (9,5) indicate that creep is not occurring along this section of the fault. In addition, the San Andreas fault within the Palmdale uplift has been almost aseismic for the past forty years. An increase in low-level earthquakes ($\leq M_L = 3$), however, has been reported for 1976 and 1977 by McNally and Kanamori (8). Models for strike-slip faults indicate that a modification of regional stress trajectories should occur near a locked fault (1).

To test for the effect of the locked San Andreas fault on the regional stress field, we made 29 in situ measurements at eight sites along a broad profile perpendicular to the San Andreas fault, southeast of Palmdale (Figure 1). Stress orientations were measured using a strain relaxation technique that employs a strain cell similar to the one described by Stephenson and Murray (13) and Leeman (7). This strain cell is commonly known as the "doorstopper".

EXPERIMENTAL TECHNIQUES

Our transducer consists of a hard plastic cylinder which contains a low modulus plastic, Silguard, above Dow-Corning RTV. At the base of the RTV is a foil-resistance strain-gauge rosette with gauges spaced 120° apart. A thermal compensation gauge is embedded in the Silguard above the RTV. The resistance of the compensation gauge is balanced against that of the active components of the rosette using an AC resistance bridge.

The strain gauge rosette is exposed at the end of the transducer and is epoxyed to the flattened bottom of a borehole. When bonded, each gauge covers an area of 21 mm^2 between 1 and 8 mm measured from the center of the core along a radius. See

[1]Lamont-Doherty Geological Observatory Contribution No. 2643

19th U.S. Symposium on Rock Mechanics, 1978, Stateline, Nevada; p. 95-100.

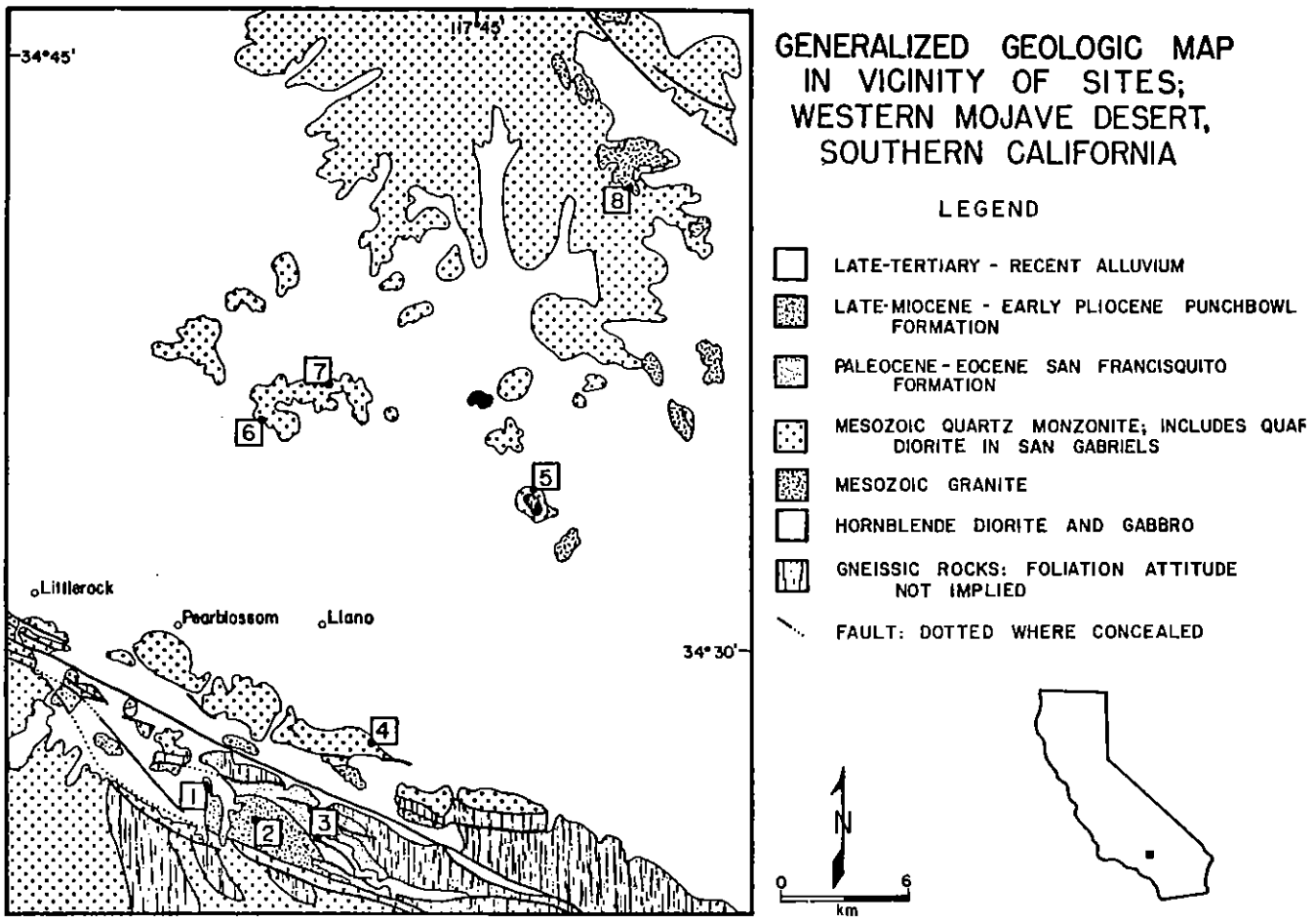

Figure 1. Map of generalized geology in the vicinity of in situ stress measurement sites, western Mojave Desert, and foothills of the San Gabriel Mountains. The sites are numbered. The longest continuous fault in the southern part of the map is the San Andreas. The Punchbowl fault and various subsidiary faults are also shown. Geology simplified from Dibblee (2).

Jaeger and Cook (6; Figure 15.5, p. 371) for a cross-section of a transducer and borehole after overcoring. We used a NW oversize diamond bit (79 mm outer diameter), which produced a 55 mm core, for drilling both the initial hole and the overcore. Two boreholes were drilled at each site with two or three measurements in each at depths ranging from 0.5 to 3 m. Our technique is similar to Stephenson and Murray's (13) where a cable runs from the doorstopper through the drill string to our strain indicator to allow readings during overcoring. This enables us to recover data even if the core broke before the drilling was completed. We calculated the maximum and minimum principal strain (ε_1 and ε_2, respectively) and their orientation from the strain observed on the three gauges of the rosette.

To transform strain to stress, we measured a mechanical property similar to linear compressibility, defined by Nye (10, p. 146): "The linear compressibility of a crystal is the relative decrease in length of a line when the crystal is subjected to unit hydrostatic pressure." This definition applies to a uniform three-dimensional load. Because in our experiment the sample is stressed radially, but is not constrained axially, we refer to the relation between stress to strain, as the "pseudo-linear compressibility" (PLC).

The measurements of PLC are done in the field using a cylindrical test chamber on cores with doorstoppers still attached [see Sbar, Engelder, Plumb, and Marshak (12); Figure 2]. A uniform radial stress was applied to the core incrementally from zero to about 40 bars, and was then returned incrementally to zero. This was done twice for each sample. We observed a nonlinear relation between load and strain, and only a partial recovery of the strain upon removing the stress. Due to the inelastic behavior of the samples, particularly upon overcoring, there are undoubtedly errors in the magnitude of PLC used in the stress calculation. Throughout all cycles, however, the direction of maximum PLC varied ± 5°, so the calculated stress orientations do not incorporate large errors due to inelasticity. We arbitrarily used the PLC measured at 13.6 bars for most of our calculations of stress.

The PLC is related to the strain (ε_i) measured during radial compression and to the known pressure (P) applied by the cylindrical test chamber, by the formula:

$$PLC = \frac{\varepsilon_i}{P} = \frac{1-\nu_i}{E_i} \qquad (1)$$

Where ν_i is Poisson's ratio, and E_i is Young's modulus for stress applied parallel to ε_i (Jaeger and Cook, 6, p. 134). In the above, two-dimensional orthorhombic symmetry is assumed.

All of our cores are anisotropic to some degree, as shown by the variation of PLC with direction. Using the value of PLC parallel to each of the three gauges of the strain rosette, we can transform the strain measured on each gauge during overcoring to the stress which was exerted parallel to that gauge prior to overcoring by the formula:

$$\sigma_{oc} = \frac{\varepsilon_{oc}}{PLC} \qquad (2)$$

where ε_{oc} is the strain that occurred during overcoring and σ_{oc} is the corresponding stress. Effectively, this is a transformation from tensor strain to tensor stress which, to a first approximation, incorporates the anisotropy of the sample. From the three components of stress, the principal stresses and their orientations may be easily calculated.

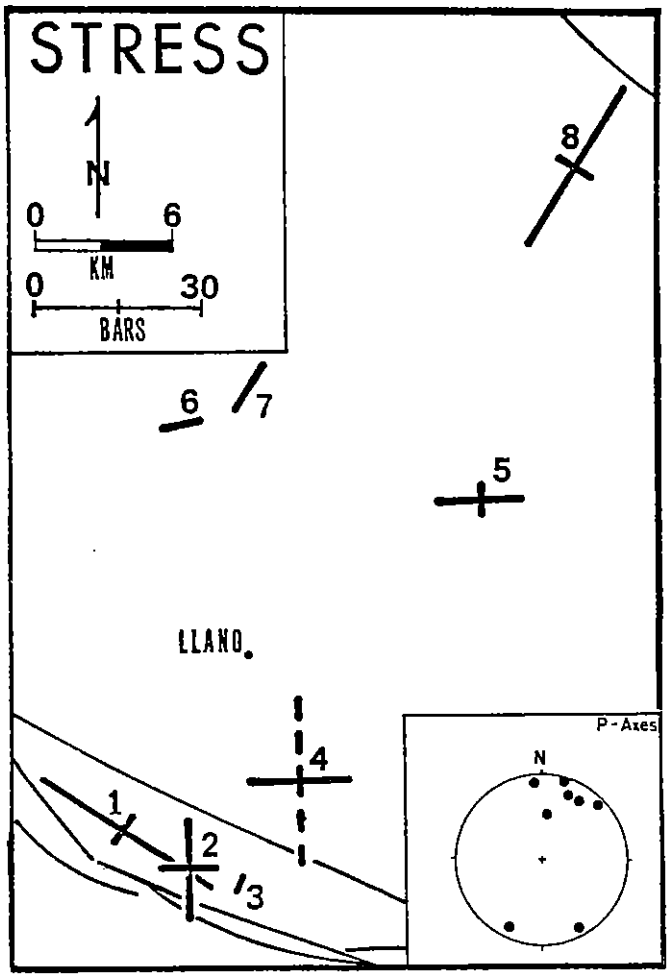

Figure 2. Tensor averages of the maximum and minimum horizontal stress at each site. Dashed lines indicate tensional stress. The map covers the same area as Figure 1. A lower hemisphere equal-area projection of P-axes (compressional axes) for fault-plane solutions in southern California is shown in the lower right-hand corner. Sources of these data are listed in Sbar, Engelder, Plumb and Marshak (12).

Equation (1) is exact for a radial load, but the stresses exerted on the rock in the field are not equal in all directions. Thus, there is an error inherent in the transformation from stress to strain. Fortunately, this error does not significantly change the calculated orientation of the

Table 1. Strain, material properties, and calculated stress for all overcores

SITE #	HOLE	DEPTH	STRAIN				PSEUDO-LINEAR COMPRESSIBILITY					STRESS		
			ε_1	ε_2	Azimuth of ε_1	Ratio	Applied Pressure	Max $bars^{-1}$	Min $bars^{-1}$	Azimuth of Max	Anisotropy	σ_1	σ_2	Azimuth of σ_1
		cm	$\times 10^{-6}$	$\times 10^{-6}$			bars	$\times 10^{-6}$	$\times 10^{-6}$			bars	bars	
1	A	71	708	409	N67°W	1.7								
		201	1098	413	N59°W	2.7	17	54.6	18.8	N52°E	65%	37.9	2.7	N54°W
		279	1060	484	N48°W	2.2	13.6	26.6	18.2	N15°E	31%	44.4	13.2	N56°W
	B	79	862	706	N78°W	1.2								
		137	966	316	N64°W	3.1	13.6	72.7	31.5	N23°E	57%	24.2	0.4	N62°W
	AVERAGE		930	475	N60°W	2.0		49.4	24.8	N34°E	50%	35.4	5.5	N57°W
2	A	91	534	353	N16°W	1.5	14.3	41.9	21.0	N78°W	50%	19.0	5.7	N - S
		147	762	345	N 8°W	2.2	17	33.5	25.8	N13°W	23%	18.6	11.4	N 8°W
	B	107	391	313	N46°E	1.2	15.3	28.0	17.8	N18°W	36%	16.1	9.5	N 9°W
	AVERAGE		544	355	N 7°W	1.5		32.2	23.8	N76°W	26%	17.8	9.1	N - S
3	A	58	72	-33	N22°E									
		89	65	-49	N25°E		13.6	14.7	12.4	N58°E	16%	4.0	-2.9	N24°E
	B	79	71	- 2	N39°E		13.6	23.9	16.8	N35°W	30%	3.3	-0.1	N44°E
		104	9	-28	N33°E		13.6	17.0	12.4	N 7°W	27%	0.6	-1.5	N32°E
	AVERAGE		71	-32	N23°E			17.6	14.8	N21°W	16%	2.5	-1.4	N31°E
4	A	46	394	-890	N89°E		13.6	22.4	13.2	N 1°W	41%	15.7	-31.7	N88°E
		64	124	73	N86°W									
	B	150	544	76	N63°W									
	AVERAGE		327	-220	N84°W			22.4	13.2	N 1°W	41%	15.7	-31.7	N88°E
5	A	120	300	168	N81°E	1.8								
	B	71	454	77	N84°E	5.9	13.6	30.6	24.2	N76°E	21%	12.5	2.7	N87°E
		152	1356	15	N69°E	90.6								
		188	142	-67	N81°E									
	AVERAGE		556	55	N74°E	10.1		30.6	24.2	N76°E	21%	12.5	2.7	N87°E
6	A	147	100	2	N63°E	50	13.6	12.4	6.3	N32°E	49%	7.6	1.2	N70°E
		213	134	37	N80°W	3.6	13.6	17.4	12.4	N14°E	29%	8.6	1.8	N76°W
	B	152	60	-45	N55°E		13.6	7.8	6.2	N49°E	23%	6.3	-4.8	N54°E
		203	86	7	N81°E	12.3	13.6	13.2	6.7	N30°E	49%	8.0	0.8	N84°W
	AVERAGE		86	9	N73°E	9.6		12.6	8.0	N28°E	37%	6.6	0.7	N78°E
7	A	152	157	-20	N 2°E									
		226	253	42	N 1°E	6.0	13.6	24.1	10.2	N 8°E	57%	8.9	4.7	N 7°W
	B	183	124	-63	N40°E		13.6	10.1	9.3	N22°E	9%	1.0	-5.2	N40°E
	AVERAGE		160	4.2	N13°E	38.1		17.1	9.8	N 9°E	43%	8.7	0.7	N32°E
8	A	71	132	35	N15°E	3.8	13.6	4.5	2.4	N30°W	47%	32.9	8.2	N34°E
	B	107	111	-17	N24°E									
		170	75	33	N 7°E	2.3								
	AVERAGE		105	18	N18°E	5.8		4.5	2.4	N30°W	47%	32.9	8.2	N34°E

ε_1 and ε_2, σ_1 and σ_2 are principal strains and stresses, respectively. Ratio is max/min. Anisotropy is (max-min)/max. The applied pressure is the radial stress at which the pseudo-linear compressibility was measured. All of the averages are tensor averages.

principal stresses, although it does affect their magnitude.

A further correction must be applied to the stress data to account for the concentration of stress that occurs at the end of a borehole. We used an experimentally derived correction suggested by Leeman (7):

$$\sigma_i = \sigma_i' + 0.75\ (0.645 + \nu)\ \sigma_z \qquad (3)$$

where σ_i is one component of the applied stress in the earth, σ_i' is the stress computed from strain relaxation at the end of a borehole, ν is Poisson's ratio (which we take as 0.25), and σ_z is the vertical stress assumed to equal density times gravitational acceleration times depth. This correction does not change the direction of the principal stresses. Once we applied all of the corrections, we calculated tensor averages for all the reliable stress and strain measurements at a given site (Table 1).

DATA

We made 29 successful strain relaxation measurements over the course of one month in the field. Usually six measurements were attempted at each of

the eight sites, but failures occurred because of fractures beneath or near the gauges and because of separation of the wires from the gauge. Because we did not always obtain the 10 cm length core necessary for mechanical tests, only eighteen stress calculations could be made. All our data - strain relaxation, linear compressibility and stress - are tabulated in Table 1.

The variation in orientation of the principal strains at the individual sites ranges from 15° to 45° for measurements where the ratio of maximum to minimum strain is greater than 1.5. The variation in orientation of the maximum PLC at the individual sites is 35° to 79°, for cores with mechanical anisotropies greater than 15%. This is slightly greater than the variation in orientation for the principal strains. As might be expected, the sites with the greatest anisotropy had the least variation in orientation of maximum PLC, and vice-versa. In general, the ratio of maximum to minimum PLC was lower than the ratio of maximum to minimum strain. The anisotropy of the cores varied from 9% to 65%.

At sites 7 and 8, farthest from the San Andreas fault, σ_1 (tensor average) trends NNE (Figure 2). At sites 4, 5, and 6 the next closest on the northeast side, σ_1 trends ENE to east-west. Sites 1, 2, and 3 southwest of the fault show a rotation of from N60°W parallel to the fault to N30°E going from northwest to southeast. All three sites were equidistant from the trace of the 1857 fault break on the San Andreas.

INTERPRETATION

The strain relaxation observed at a site is influenced not only by regional tectonic stress, but also by topographic stress, residual stress, and the degree of outcrop coupling across fractures. One of the difficulties of near-surface strain relaxation measurements is the estimation of the relative contributions of regional tectonic stress and noise sources for each measurement.

Residual stress is locked into a rock during the course of its thermal, tectonic, and burial history. Its presence can be determined by double overcoring where a second overcore is drilled within the first. The strain measured during the second overcore represents residual stress because the core has already been relieved of all applied stress. Time constraints allowed us to make double overcores only in the sedimentary rocks of site 1. No significant residual stress was observed.

Both topographic and regional tectonic stress are applied rather than residual. Topography may add a component of stress to the regional tectonic stress in two ways. First, lithostatic loading at the base of hillslopes can cause a Poisson expansion that is perpendicular to the mountain front or the axis of a valley (6, p. 356-358). Second, the slope of valleys causes a concentration of tectonic stress perpendicular to the valley axis (4). Sites 3, 4, and 5 were adjacent to steep-sided slopes; of these, sites 3 and 4 were in valleys. Only at site 4 was σ_1 perpendicular to a valley axis. Topographic stress may be superimposed on the tectonic stress at sites 3 and 5, although σ_1 was not perpendicular to the slopes in either case. From our measurements it is difficult to quantify the effect topography had on the in situ stress measured at sites 3, 4, and 5.

Coupling of the outcrop on which the measurements are made to the earth is a problem which appears to affect the magnitude and possibly the direction of the stress observed. Engelder and Sbar (3) found that the magnitude and reproducibility of surface strain relaxation measurements in northern New York appeared to be directly proportional to the horizontal dimensions of blocks bounded by vertical joints. If coupling across horizontal joints were a significant problem, we would expect a noticeable difference in measurements above and below sheet fractures. This was not observed in our data.

The mechanical properties of strata below the outcrop may also weaken the coupling to earth strain at depth. The formation at site 3 is a sequence of interbedded sandstones and shales. Since we observed very low stress there (Figure 2 and Table 1), we suspect that coupling may have been poor across the shaly layers.

The variation in magnitude of the principal stresses from site to site as shown in Figure 2 may not represent a real variation in the stress at depth, but may be a function primarily of the coupling of the outcrop to the earth. The largest magnitude for the maximum compressive stress (σ_1) is about 35 bars. This may represent the true lower limit for the near-surface stress which might be extrapolated to depth to find the state of stress near the San Andreas fault.

T. Tullis (14) made strain relaxation measurements, using the U. S. Bureau of Mines borehole deformation gauge, at four sites near ours. His results are quite similar to ours both in orientation of principal stresses and in the variation of magnitude from site to site. Because of this similarity we feel confident that our results are not an artifact of our measurement technique and that the interpretation of these data in terms of tectonic stress is valid.

The goal of this research is to determine if we can measure the regional tectonic stress and its modification in the vicinity of a fault with a high earthquake potential. Such modification can be caused by buildup of strain across the fault, by the geometry of the fault, and by local strain release in the form of earthquakes. Parameters such as residual stress and topographic stress are, in essence, "noise" which may obscure the tectonic stress.

At sites 3, 7, and 8, σ_1 is oriented NNE, approximately parallel to the regional tectonic stress inferred from fault-plane solutions (Figure 2). Such an orientation is understandable for sites 7 and 8 which were distant from the fault and might not be influenced by the presence of the fault.

Our measurements show that as the fault is approached from the north side there is a clockwise rotation of σ_1 from NNE at sites 7 and 8 to about N70-75°E at sites 5 and 6 to N84°W at site 4. South of the fault, in the fault zone, our 3 measurements were equidistant from the fault. They indicate a rotation of σ_1 from N60°W at site 1 to NNE at site 3. The agreement of Tullis' data (14) and ours with the regional stress inferred from fault-plane solutions suggests that both techniques did record the actual near-surface stress field. Our measurements near the fault indicate a complexity in the stress field. This is supported by the unusual localized region of low-level seismicity reported at Juniper Hills by McNally and Kanamori (8) just to the northwest of site 1. The fault-plane solutions they determined indicate thrust faulting with no significant strike-slip component and a variation of compression axes by as much as 90°.

CONCLUSIONS

Our in situ stress measurements far from the fault appear to reflect the regional tectonic stress field as inferred from fault-plane solutions and geologic structures. Near the fault, our principal stress orientations deviate considerably from the regional trend. Thus, we might infer that the stress orientations we observed were indicative of influence by the fault on the regional stress field. Other near-surface strain relaxation measurements in the same area (Tullis, 14) are consistent in orientation and magnitude with our measurements.

The doorstopper technique is relatively fast and inexpensive. It can work in areas inaccessible to hydrofracture equipment and in rocks too fractured for work with the U. S. Bureau of Mines technique. Our pilot study has shown that tectonic stress can be detected by near-surface in situ stress measurements.

ACKNOWLEDGEMENTS

We acknowledge the assistance by Tony Lomando in fabricating the doorstoppers used in this experiment. Terry Tullis helped us in the field logistics. Christopher Scholz and Roger Bilham critically reviewed the manuscript. This research was supported by the U. S. Geological Survey under grant number 14-08-0001-0417 to the University of Arizona and 14-08-0001-0404 to Lamont-Doherty Geological Observatory.

REFERENCES

1. Barber, D. W., and G. M. Sowers, 1974, A photoelastic study of the effects of surface geometry on fault movements, in Advances in Rock Mechanics, Proc. 3rd Congress, Internat. Society Rock Mech., 585-590.

2. Dibblee, T. W., Jr., 1967, Areal geology of the western Mojave Desert, California, U. S. Geol. Survey Prof. Paper 522, 153 p.

3. Engelder, T., and M. L. Sbar, 1977, The relationship between in situ strain relaxation and outcrop fractures in the Potsdam sandstone, Alexandria Bay, New York, Pure and Applied Geophys., 115, 41-55.

4. Harrison, J. C., 1976, Cavity and topographic effects in tilt and strain measurements, J. Geophys. Res., 81, 319-328.

5. Hofmann, R. B., 1968, Geodimeter fault movement investigations in California, Calif. Dept. Water Resources Bull. 116, Pt. 6, 183 p.

6. Jaeger, J. C., and N. G. W. Cook, 1969, Fundamentals of Rock Mechanics, Chapman and Hill, London, 515 p.

7. Leeman, E. R., 1971, The C.S.I.R. "doorstopper" and triaxial rock stress measuring instruments, Rock Mechanics, 3, 25-50.

8. McNally, K., and H. Kanamori, 1977, Unusual seismic activity along the San Andreas fault near Palmdale, southern California, EOS, Trans. Am. Geophys. Union, 58, 1120.

9. Meade, B. K., and J. B. Small, 1966, Current and recent movement on the San Andreas fault, Calif. Div. Mines and Geo. Bull. 190, 385.

10. Nye, J. F., 1957, Physical Properties of Crystals, Oxford Univ. Press, London, 322 p.

11. Prescott, W. H., and J. C. Savage, 1976, Strain accumulation on the San Andreas fault near Palmdale, California, J. Geophys. Res., 81, 4901-4908.

12. Sbar, M. L., T. Engelder, R. Plumb, and S. Marshak, 1978, Stress pattern near the San Andreas fault, Palmdale, California, from near surface in situ measurements, J. Geophys. Res., 83, in press.

13. Stephenson, B. R., and K. J. Murray, 1970, Application of the strain rosette relief method to measure principal stress throughout a mine, Int. J. Rock Mech. Min. Sci., 7, 1-22.

14. Tullis, T. E., 1977, Stress measurements in shallow overcoring on the Palmdale uplift, EOS, Trans. Am. Geophys. Union, 58, 1122.